Probing quantum walks through coherent control of high-dimensionally entangled photons

Poolad Imany,[1,2,]† Navin B. Lingaraju,[1,2] Mohammed S. Alshaykh,[1,2] Daniel E. Leaird,[1,2] Andrew M. Weiner[1,2]

[1]School of Electrical and Computer Engineering, Purdue University, West Lafayette, IN, USA.

[2]Purdue Quantum Science and Engineering Institute, Purdue University, West Lafayette, IN, USA.

† pimany@purdue.edu

Summary

Demonstration of continuously tunable photonic quantum walks in the frequency domain with high-dimensionally entangled photon pairs.

Abstract

Quantum walks in atomic systems are especially well-suited for the simulation of many-body physics and can potentially offer an exponential speedup in solving certain black box problems. The ability to control the duration of a walk unlocks its full potential for quantum search algorithms and quantum simulation. Photonics offers an alternate route to simulating such nonclassical behavior in a more robust platform. However, in implementations to date, any change to the effective duration of a photonic quantum walk has required some modification of the device or system footprint. Here we report quantum walks of biphoton frequency combs where the duration of the walk, or circuit depth, is tunable over a continuous range without any change to the physical dimensions of the system. The walkers in our platform are discrete frequency modes and the coupling between these modes is mediated by electro-optic modulation of the waveguide refractive index. Through control of the phase across different modes, we demonstrate a rich variety of behavior: from walks exhibiting ballistic transport or strong energy confinement, to subspaces featuring scattering centers or local traps. We also explore the role of entanglement dimensionality in the creation of energy bound states, which illustrate the potential for these walks to quantify entanglement in high-dimensional systems.

INTRODUCTION

A quantum particle can exist in a superposition of paths, or modes, and interference between the probability amplitudes of these outcomes results in phenomena unique to random walks of quantum systems (*1*–*3*) – enhanced propagation, otherwise called ballistic transport (*4*), or Anderson localization, where the wavefunction becomes confined in a disordered system (*5*, *6*). Quantum walks of two or more particles can exhibit nonclassical phenomena such as bunching or antibunching for bosons and fermions, respectively (*7*). The complex dynamics observed in such walks cannot be explained by classical models and, therefore, can serve as a probe of entanglement or interactions between particles (*1*, *7*–*11*). Owing to the variety of nonclassical behavior they can exhibit, quantum walks have the potential to provide a dramatic speed up in certain computational tasks like physical database searches (*12*) and tests of graph isomorphism (*13*).

Quantum walks come in two flavors – continuous and discrete (*14*). Discrete-time quantum walks can evolve through a sequence of discrete events characterized by a "coin flip" that scatters the walker into adjacent modes. In continuous-time quantum walks, the state evolves through continuous tunneling to neighboring modes. Such walks have been observed in atomic systems (*1*) and their depth is determined by the evolution time of the quantum state. Continuous evolution of the quantum state, coupled with the ability to choose an arbitrary walk duration, allows one to explore a wide range of parameter space. Consequently, these walks are especially well-suited to simulating Hamiltonian dynamics (*9*) and solving certain black box problems exponentially faster (*15*). To achieve even comparable performance with discrete quantum walks, additional system complexity is required, primarily through an extra degree of freedom (*14*).

Walks of correlated particles have also been implemented in photonic systems as they offer a more robust platform in terms of decoherence and room-temperature operation (*2*, *3*, *9*, *16*, *17*). However, photonic quantum walks demonstrated to date suffer from the drawback that their circuit depth can only be incremented by physically altering the footprint of the system. Here we report continuous quantum walks with photon pairs entangled across multiple, discrete frequency modes (*8*, *18*) where the effective duration of the walk is fully tunable without necessitating any physical change to the system. With arbitrary control of the phase across different modes, we demonstrate walks exhibiting enhanced ballistic transport or strong energy confinement, as well as subspaces featuring scattering or trapping of two-photon correlations. We also explore the role of entanglement dimensionality in creating energy bound states – states whose energy remains unaltered over the duration of a walk – and show that their sensitivity to multilevel entanglement hints at the potential for such walks to quantify entanglement in high-dimensional systems.

FREQUENCY DOMAIN QUANTUM WALKS WITH TUNABLE DEPTH

A photon can "walk" across different modes in any one of its many degrees of freedom, whether it be time (*2*, *3*), path (*8*, *16*, *17*, *19*), orbital angular momentum(*20*), or frequency (*21–23*). All that is required to observe such behavior is the presence of coupling between different modes in the particular degree of freedom. In the case of a quantum walk in the frequency domain, this coupling is mediated by a periodic (temporal) modulation of the waveguide refractive index. Such coupling, or mode-splitting, can be realized in electro-optic phase modulators driven with a single sinusoidal radiofrequency (RF) tone. The effect of this perturbation is that the wavefunction of a photon traversing the waveguide picks up a factor of $e^{i\delta \cos \omega_{\mathrm{m}} t}$. Here, δ corresponds to the strength of the modulating RF field and ω_m denotes the frequency of this RF modulation. Viewed from the perspective of the frequency domain, phase modulation scatters a single frequency into a comb-like spectrum with adjacent frequency modes separated by ω_{m} in frequency [Fig. 1a]. The amplitude of a comb line a distance $n\omega_{\mathrm{m}}$ away from the original frequency is given by n$^{\mathrm{th}}$-order Bessel function $J_n(\delta)$. In analogy to quantum walks based on path encoding, the depth of such a frequency domain quantum walk can be incremented simply by cascading one modulator after another. However, a particular strength of the frequency domain approach is that a cascade of n identical phase modulators is equivalent to increasing the strength of the modulating RF field in a *single* modulator by this factor of n. In other words, the depth of the walk can be tuned over a *continuous* range by simply modifying the strength of the modulating RF field. This is in contrast to quantum walks in the spatial domain where evolution of the state is determined by propagation length (*9*, *24*).

Fig. 1a shows results from quantum walks of a single photon that starts out in a single frequency

mode. As the strength of the modulating RF field (δ) increases, the extent to which the input mode scatters to outer frequency modes also increases. In Fig. 1a, the output photon distribution is plotted as a function of modulation strength δ, which in our platform is equivalent to the effective walk duration. The "rabbit ears" observed in this distribution signify the presence of ballistic energy transport – a signature of random walks with quantum systems. In particular, the standard deviation of the output photon distribution grows linearly with δ (*25*). For a classical random walk, transport to neighboring modes is not nearly as fast and its standard deviation grows only as $\sqrt{\delta}$ (*25*).

Quantum walks of entangled particles, particularly those featuring high-dimensional entanglement, exhibit a richer variety of behavior than is possible with just a single photon occupying a single frequency mode. To explore the effect of entanglement on quantum walks in the frequency domain, we studied the evolution of two-photon quantum frequency combs, commonly referred to as biphoton frequency combs (BFCs) [Fig. 1b], as they traverse the system.

QUANTUM WALKS AND MULTI-LEVEL ENTANGLEMENT

BFCs have been generated directly in on-chip optical microresonators (*26–29*) or carved from continuous down-conversion spectra (*30*). For results reported here, BFCs were generated by the latter approach as it allows flexibility in the choice of comb linewidth (Δλ) and free spectral range (FSR). Broadband time-energy entangled photons (~5 THz) were generated by type-0 down-conversion in a periodically-poled lithium niobate waveguide (PPLN). In this process, a pump photon from a continuous wave laser (~775 nm) is converted into a pair of daughter photons in the telecommunications band (~1520-1580 nm). As energy is conserved in this process, the energies (frequencies) of the daughter photons must add up to that of the pump photon. In other words, the two photons in an entangled pair are anticorrelated in frequency. This two-photon spectrum is carved into a BFC using a Fourier transform pulse shaper. The 3dB linewidth of each frequency mode is set to 9 GHz – the resolution limit of our pulse shaper. To ensure minimal crosstalk between adjacent modes, the FSR of the BFC is chosen to be 25 GHz.

The pulse shaper is used to not only manipulate the amplitude of the biphoton spectrum, but also its phase prior to any quantum walk. In particular, the spectral phase can be set to vary continuously or to make discrete jumps from one mode to the next. Once the desired state has been prepared, it is sent to an electro-optic phase modulator that implements the mode-mixing operations which give rise to a quantum walk. Our modulator is driven with a 25 GHz sinusoidal RF waveform, identical to the FSR of the BFC, with the RF power tunable over a continuous range. Downstream of the modulator is a second pulse shaper, which selects a pair of output frequencies and routes each one to a superconducting nanowire single-photon detector (SNSPD). Two-photon events between different frequency modes are identified by correlations in their arrival time and this data is used to construct a measurement of the joint spectral intensity (JSI) of the BFC – a two-photon correlation map that illustrates the effects of a quantum walk in energy (frequency) space.

Enhanced ballistic energy transport

As noted earlier, one hallmark of a quantum walk is the observation of ballistic energy transport of the quantum state across modes of the system. We demonstrate even stronger transport for the case of a BFC entangled across eight dimensions and having the form $|\psi\rangle = 1/\sqrt{8}\ \sum_{m=1}^{8}|m,-m\rangle_{\mathrm{SI}}$, where S and I denote the signal (high-frequency) and idler (low-frequency)

photons, respectively. The JSI of this state, i.e., in the absence of any RF modulation, is completely anticorrelated in frequency [Fig. 2a]. Each pixel on the antidiagonal corresponds to the same two-photon energy, i.e., the sum of mode indices of any pixel on this line is zero. Note that the sum of the mode indices on any line parallel to the antidiagonal is a constant and corresponds to a different value for the total energy of the two-photon state. In Fig. 2b we show the JSI of this state after a quantum walk when the modulator is driven to a depth $\delta = 4.6$ (see supplementary material for the JSI measurements at various modulation depths). Experimental data clearly show diffusion, or transport, of two-photon correlations away from the original JSI, which matches results expected from theory (see supplementary material). Transport perpendicular to the sum-frequency axis (antidiagonal) and toward the top right corner of the JSI corresponds to events where the overall energy of the biphoton increases, i.e., the modulator transfers energy to the two-photon state. The converse, when the biphoton transfers energy to the modulator, manifests as transport toward lower left corner of the JSI. In other words, what we observe is two photons experiencing the same frequency shift, which resembles, but is qualitatively different from, bosonic bunching (Hong-Ou-Mandel interference) in the frequency domain (*31*).

To quantify this energy transfer, we tabulate the total number events along the antidiagonal, as well as along each line parallel to the antidiagonal, to determine to the probability of a biphoton exiting the system with a particular total energy. Energy transfer between the quantum circuit and the two-photon state, expressed in terms of the sum of photon mode indices, is plotted in Fig. 2d as a function of modulation depth δ. The standard deviation of the biphoton energy at the output, as in the single photon case, is linear with δ [Fig. 5a]. However, this linear rate of energy transfer is roughly twice as fast in the case of entangled photons. Such enhanced energy transport was previously demonstrated with high-dimensional, path-entangled photon pairs (*8*).

Energy bound state

We break new ground in photonic quantum walks by demonstrating the opposite of ballistic energy transport – strong confinement of the biphoton energy. To achieve this, we modify the spectral phase of the BFC to create a state of the form $|\psi\rangle = 1/\sqrt{8}\ \sum_{m=1}^{8} e^{im\pi}|m,-m\rangle_{\mathrm{SI}}$, i.e., a state in which adjacent modes have a π phase with respect to one another. This operation can be viewed as a linear spectral phase ramp, which is equivalent to delaying one photon with respect to its entangled counterpart by half the modulation period. As a result of this delay, photons in an entangled pair acquire *equal but opposite* frequency shifts. This is clearly illustrated in the JSI measurement after a quantum walk [Fig. 2c], which shows that frequency correlations remain largely confined to the antidiagonal of the JSI measurement. In other words, the energy of the two-photon state is mostly unchanged. As the duration of the walk (modulation depth δ) increases, frequency correlations merely propagate outward along the antidiagonal to include new combinations of high and low photon energies [see Fig. S3]. However, this energy gain or loss is correlated within a photon pair. If the idler gains some energy, the signal loses that same amount of energy with the result that the total energy of the state is preserved.

Time domain perspective

The evolution of the biphoton, as depicted by two-photon correlation maps [Figs. 2b, c], can also be understood from a time-domain illustration of the quantum walk that considers the effect of electro-optic phase modulation on the time correlation function of entangled photons (*32*). In Fig. 4, the strength of the modulating RF waveform is shown (in blue) as a function of time. The signal

photon, which can arrive at the modulator at any time owing to the random nature of the pair generation process, is designated by a blue arrow. In Fig. 4 we only show one possible arrival time. Here, for example, the signal reaches the modulator when the phase of the modulating RF waveform is $\pi/6$. While the idler photon also reaches the modulator at a random time, its arrival is highly correlated with that of the signal photon. This correlation is characterized by a distribution of possible values for the delay between signal and idler. The distribution, in delay space, is given by the Fourier transform of the complex biphoton spectrum (*33*). Consequently, for a narrowband biphoton spectrum with entanglement across a limited number of dimensions ["8-dimensional entanglement" in Fig. 4], there is wide range of possible values for the relative delay between signal and idler. As the entanglement dimensionality of the state increases, i.e., as the biphoton spectrum gets broader, the distribution of possible delays gets narrower ["64-dimensional entanglement" in Fig. 4]. The discretization of the biphoton spectrum in frequency space, owing to its comb-like structure, results in a distribution of relative arrival times that repeats at integer multiples of the inverse comb FSR. Since the spacing between comb lines matches the frequency of the RF waveform, this repetition of the distribution in arrival times occurs at *integer* multiples modulation period. The net effect is that both photons "see" nearly the same phase modulation slope ($d\phi/dt$), which means they experience correlated instantaneous frequency shifts (*34*) ["Correlated quantum walk" in Fig. 4].

For the energy bound state, the situation is slightly different. Here there is a π phase difference between adjacent comb lines, which corresponds to a linear spectral phase ramp or simply a time delay. This time delay corresponds to exactly half the RF modulation period. In other words, the distribution in the relative arrival of signal and idler is now spaced at *half-integer* multiples of the modulation period. Here, unlike in the case of ballistic transport described earlier, photons in an entangled pair experience anticorrelated instantaneous frequency shifts ["Anticorrelated quantum walk" in Fig. 4], which manifests through confinement of two-photon correlations to the antidiagonal (sum-frequency axis) of a JSI measurement.

Controllable diffusion in energy subspaces

The cases of enhanced ballistic scattering [Fig. 2b] and energy confinement [Fig. 2c] are a good illustration of the role spectral phase plays in the evolution of two-photon correlations. While the diffusion of correlations along, or perpendicular to, the antidiagonal represent the most straightforward forms of transport, they encompass but a subset of possible behavior that one can observe. For example, by preparing BFCs with quadratic spectral phase, we observe remarkable features in two-photon correlations – distinct energy subspaces featuring ballistic scattering or energy confinement. Figs. 3a, b show results from such quantum walks with a 16-dimensional entangled state. Increasing the number frequency modes across which the photons are entangled (16 compared to 8 in preceding experiments) allows us to clearly delineate regions exhibiting correlated energy transfer (scattering) from those exhibiting anticorrelated energy transfer (confinement). In Fig. 3b, we employ an additional linear phase pattern, reduce the dispersion, and increase the modulation depth to pin a single site where correlations are "trapped" to the center of the JSI.

While the two-photon correlation maps in Figs. 3a, b employ quadratic spectral phase, one can certainly employ more complex spectral phase patterns to engineer the features of quantum walks. As a result, the relative delay between the photon pair is controlled by the frequency derivative of the biphoton spectral phase in each frequency subspace. In other words, each input frequency mode

pair, or lattice point, exhibits modified scattering amplitudes that depend on the relative phase of the modulating RF waveform. This allows one to simulate certain features of walks with inhomogeneous potentials.

Effects of high-dimensional entanglement

The critical role played by spectral phase hints at strong differences between quantum walks featuring coherent superpositions of multiple frequency pairs $|m, -m\rangle_{\mathrm{SI}}$ as compared to mixtures of those same frequency pairs. While both states possess identical frequency correlations, in the latter the relative phase between any two basis states ($|m, -m\rangle_{\mathrm{SI}}$ and $|m', -m'\rangle_{\mathrm{SI}}$ for $m \neq m'$) is completely random. To simulate the effect of this random phase, we construct a JSI measurement of the mixed state by adding together JSI measurements resulting from quantum walks of individual frequency pairs $|m, -m\rangle_{\mathrm{SI}}$ for $m = 1, \ldots, 8$ (see supplementary material). A clear effect of incoherence is that two-photon correlations are smeared out without any sharp or well-defined features [Fig. 3c].

These results, taken together with walks presented earlier, suggest that the total energy of the two-photon state after a quantum walk can serve as an indicium of the coherence between frequency mode pairs. One metric to quantify this is the standard deviation of biphoton energy measured at the output. This is presented in terms of the mode index (single-photon case) and the sum of mode indices (two-photon case), as function of walk duration, in Fig. 5a. We see a clear indication of enhanced energy transfer for the two-photon state. In the limit of infinite multi-level entanglement, energy transfer increases at twice the rate for two-photon correlations compared to the single-photon quantum walk since both photons experience exactly the same frequency shift.

To elucidate the effect of the entanglement dimensionality, we present data for biphoton energy transfer in the cases of enhanced ballistic scattering [Fig. 5c] and strong energy confinement [Fig. 5d]. Fig. 5b shows how the standard deviation of the output biphoton energy changes as the degree of multi-level entanglement increases for a fixed walk depth ($\delta = 6.1$). The clear change in the distribution of biphoton energies as a function of entanglement dimensionality, especially in the case of the energy bound state, point to how these results can potentially be used to certify, or even quantify, high-dimensional frequency-bin entanglement (*28*, *29*).

DISCUSSION

In this article, we have explored the use of electro-optic modulation in a waveguide to realize single-photon and two-photon quantum walks in the frequency domain. Unlike analogous systems in the spatial domain, where the effective walk duration is determined by propagation length, our spectral platform reaches arbitrary walk depths without the need for any physical reconfiguration of the system. All that is needed is a change in the voltage swing of the modulating RF waveform. Furthermore, our experiments were carried out primarily using commercial telecommunications equipment with little need for any specialized fabrication. Consequently, we were able to delve more deeply into the role of mode-dependent phase on two-particle quantum walks that feature multi-level entanglement.

An avenue ripe for further exploration relates to entanglement certification. The most straightforward way to certify high-dimensional frequency-bin entanglement, under the assumption of a symmetric noise model, is through a measurement of the time correlation function. However, such a measurement becomes challenging as the degree of multi-level entanglement

(and biphoton bandwidth) increases because features in the substructure of the time correlation function become finer than the timing jitter of conventional SNSPDs (~60-80 ps). Consequently, time domain techniques are limited in their ability to probe high-dimensional entanglement (*35*). While frequency mixing techniques have been developed to overcome this limitation (*28–30*), they become onerous for high-dimensional states. The quantum walks demonstrated here and energy bound states in particular show promise as a tool to probe the joint temporal correlation of broadband, high-dimensional quantum frequency combs. Our results show that the width or timing uncertainty in the time correlation function is mapped to the spread in biphoton energies at the output of a quantum walk. While a rigorous proof is needed to establish the validity of this technique for entanglement certification and quantification (*36*), these walks clearly allow one to probe temporal features in the biphoton that cannot be resolved by direct measurements.

Another key feature of our system is that the uniformity of potentials at each lattice site, i.e., the respective mode coupling coefficients, is not limited by any fabrication tolerances as it is in the case of coupled waveguide arrays. This homogeneity can be a disadvantage from the standpoint of demonstrating phenomena like Bloch oscillations and Anderson localization (*1*, *6*)– effects that stem from site-to-site variations in lattice potentials. However, quantum walks in the spectral domain can accommodate inhomogeneous potentials by using resonant structures (*22*) or loop-based architectures where an element capable of suitable frequency transformations (*37*) is updated on each roundtrip photons make through the loop. Further complexity can also be introduced by using a second degree of freedom, like the time domain, to provide a high-dimensional "coin flip" (*38*, *39*). Such walks can be used to implement quantum algorithms that certify isomorphism between two high-degree strongly regular graphs (*13*), for example.

In sum, quantum walks in the frequency domain offer an interesting and alternate route for studying quantum walk behaviors. Our spectral platform offers more versatility from the standpoints of choosing an arbitrary walk depth and manipulating the phase across all modes in states featuring a high degree of multi-level entanglement. In addition to applications directed to search (*12*) and simulation (*7*), the phenomena we demonstrated also shows potential for quantifying entanglement in high-dimensional systems.

Materials and methods

The experimental setup is depicted in Fig. 6. We use a continuous-wave 775 nm laser with about 1 mW power shining on a periodically poled lithium niobite (PPLN) crystal to generate broadband time-frequency entangled photons with about 40 nm (5 THz) bandwidth, with a power of about 5 nW. A pulse shaper is then used to carve this spectrum to make a biphoton frequency comb (BFC) with 25 GHz frequency spacing between the bins and about 9 GHz linewidth. The pulse shaper is also able to manipulate individual frequency bins' phase. One advantage to the method of state preparation described above is that since the degree of multi-level entanglement is limited by the biphoton bandwidth (~5 THz) and the resolution of the pulse shaper (~10 GHz). In other words, with an FSR of 25 GHz, one could prepare a 100-dimensional space.

The duration of the walk is determined by the strength (voltage) of the RF waveform, which in our experiments corresponded to a value of up to 6.1 radians. This determines the extent to which distant modes are coupled to one another with a crude metric being the index of the most populated mode in a single-mode and single-particle quantum walk. For the equipment used in our

experiments this index was ~5, which is comparable other platforms (3, 17, 20, 24). However, with even small upgrades to our equipment (cabling and amplifiers rated to 25 GHz) one can achieve modulation depths ~10. Furthermore, one can achieve even higher modulation depths by simply connecting more phase modulators in series as is frequently done in the case of electro-optic comb generation (40).

After making the high-dimensional entangled state, it is sent to the quantum walk circuit which is a phase modulator driven with a 25 GHz RF sinusoidal waveform. After the quantum walk, another pulse shaper picks two frequency bins at a time and sends them to superconducting single photon detectors (SNSPDs) (Quantum Opus). The relative arrival time of photons on the SNSPD pair is then monitored using an event timer (PicoQuant HydraHarp 400).

References and Notes:

1. P. M. Preiss *et al.*, Strongly correlated quantum walks in optical lattices. *Science* **347**, 1229–1233 (2015).
2. A. Schreiber *et al.*, A 2D Quantum Walk Simulation of Two-Particle Dynamics. *Science* **336**, 55–58 (2012).
3. A. Schreiber *et al.*, Photons Walking the Line: A Quantum Walk with Adjustable Coin Operations. *Phys. Rev. Lett.* **104**, 050502 (2010).
4. N. C. Harris *et al.*, Quantum transport simulations in a programmable nanophotonic processor. *Nat. Photonics*. **11**, 447–452 (2017).
5. Y. Lahini *et al.*, Anderson Localization and Nonlinearity in One-Dimensional Disordered Photonic Lattices. *Phys. Rev. Lett.* **100**, 013906 (2008).
6. A. Crespi *et al.*, Anderson localization of entangled photons in an integrated quantum walk. *Nat. Photonics*. **7**, 322–328 (2013).
7. L. Sansoni *et al.*, Two-Particle Bosonic-Fermionic Quantum Walk via Integrated Photonics. *Phys. Rev. Lett.* **108**, 010502 (2012).
8. G. Di Giuseppe *et al.*, Einstein-Podolsky-Rosen Spatial Entanglement in Ordered and Anderson Photonic Lattices. *Phys. Rev. Lett.* **110**, 150503 (2013).
9. A. Peruzzo *et al.*, Quantum Walks of Correlated Photons. *Science* **329**, 1500–1503 (2010).
10. Y. Lahini *et al.*, Quantum walk of two interacting bosons. *Phys. Rev. A*. **86**, 011603 (2012).
11. Y. Bromberg, Y. Lahini, R. Morandotti, Y. Silberberg, Quantum and Classical Correlations in Waveguide Lattices. *Phys. Rev. Lett.* **102**, 253904 (2009).
12. A. M. Childs, J. Goldstone, Spatial search by quantum walk. *Phys. Rev. A*. **70**, 022314 (2004).
13. S. D. Berry, J. B. Wang, Two-particle quantum walks: Entanglement and graph isomorphism testing. *Phys. Rev. A*. **83**, 042317 (2011).
14. A. M. Childs, On the Relationship Between Continuous- and Discrete-Time Quantum Walk. *Commun. Math. Phys.* **294**, 581–603 (2010).

15. A. M. Childs *et al.*, in *Proceedings of the thirty-fifth ACM symposium on Theory of computing - STOC '03* (ACM Press, New York, New York, USA, 2003), p. 59.

16. H. B. Perets *et al.*, Realization of Quantum Walks with Negligible Decoherence in Waveguide Lattices. *Phys. Rev. Lett.* **100**, 170506 (2008).

17. J. Carolan *et al.*, On the experimental verification of quantum complexity in linear optics. *Nat. Photonics*. **8**, 621–626 (2014).

18. A. F. Abouraddy, G. Di Giuseppe, D. N. Christodoulides, B. E. A. Saleh, Anderson localization and colocalization of spatially entangled photons. *Phys. Rev. A*. **86**, 040302 (2012).

19. Y. Lahini, G. R. Steinbrecher, A. D. Bookatz, D. Englund, Quantum logic using correlated one-dimensional quantum walks. *npj Quantum Inf.* **4**, 2 (2018).

20. F. Cardano *et al.*, Quantum walks and wavepacket dynamics on a lattice with twisted photons. *Sci. Adv.* **1**, e1500087 (2015).

21. P. L. Knight, E. Roldán, J. E. Sipe, Quantum walk on the line as an interference phenomenon. *Phys. Rev. A*. **68**, 020301 (2003).

22. C. Reimer, Y. Hu, A. Shams-Ansari, M. Zhang, M. Loncar, High-dimensional frequency crystals and quantum walks in electro-optic microcombs. *arXiv Prepr.*, arXiv:1909.01303 (2019).

23. D. Bouwmeester, I. Marzoli, G. P. Karman, W. Schleich, J. P. Woerdman, Optical Galton board. *Phys. Rev. A*. **61**, 013410 (1999).

24. T. Eichelkraut *et al.*, Coherent random walks in free space. *Optica*. **1**, 268 (2014).

25. M. Karski *et al.*, Quantum Walk in Position Space with Single Optically Trapped Atoms. *Science* **325**, 174–177 (2009).

26. C. Reimer *et al.*, Generation of multiphoton entangled quantum states by means of integrated frequency combs. *Science* **351**, 1176–1180 (2016).

27. J. A. Jaramillo-Villegas *et al.*, Persistent energy-time entanglement covering multiple resonances of an on-chip biphoton frequency comb. *Optica*. **4**, 655–658 (2017).

28. M. Kues *et al.*, On-chip generation of high-dimensional entangled quantum states and their coherent control. *Nature*. **546**, 622–626 (2017).

29. P. Imany *et al.*, 50-GHz-spaced comb of high-dimensional frequency-bin entangled photons from an on-chip silicon nitride microresonator. *Opt. Express*. **26**, 1825–1840 (2018).

30. P. Imany, O. D. Odele, J. A. Jaramillo-Villegas, D. E. Leaird, A. M. Weiner, Characterization of coherent quantum frequency combs using electro-optic phase modulation. *Phys. Rev. A*. **97**, 013813 (2018).

31. P. Imany *et al.*, Frequency-domain Hong–Ou–Mandel interference with linear optics. *Opt. Lett.* (2018).

32. C. Belthangady, S. Du, C.-S. Chuu, G. Y. Yin, S. E. Harris, Modulation and measurement of time-energy entangled photons. *Phys. Rev. A*. **80**, 031803 (2009).

33. A. Pe'er, B. Dayan, A. A. Friesem, Y. Silberberg, Temporal Shaping of Entangled Photons. *Phys. Rev. Lett.* **94**, 073601 (2005).

34. A. M. Weiner, *Ultrafast Optics* (John Wiley & Sons, Inc., Hoboken, NJ, USA, 2009; http://doi.wiley.com/10.1002/9780470473467).

35. N. B. Lingaraju *et al.*, Quantum frequency combs and Hong–Ou–Mandel interferometry: the role of spectral phase coherence. *Opt. Express*. **27**, 38683 (2019).

36. J. Bavaresco *et al.*, Measurements in two bases are sufficient for certifying high-dimensional entanglement. *Nat. Phys.* **14**, 1032–1037 (2018).

37. J. M. Lukens, P. Lougovski, Frequency-encoded photonic qubits for scalable quantum information processing. *Optica*. **4**, 8–16 (2017).

38. P. Imany *et al.*, High-dimensional optical quantum logic in large operational spaces. *npj Quantum Inf.* **5**, 1–10 (2019).

39. C. Reimer *et al.*, High-dimensional one-way quantum processing implemented on d-level cluster states. *Nat. Phys.* **15**, 148–153 (2019).

40. A. J. Metcalf, V. Torres-Company, D. E. Leaird, A. M. Weiner, High-Power Broadly Tunable Electrooptic Frequency Comb Generator. *IEEE J. Sel. Top. Quantum Electron.* **19**, 231–236 (2013).

Acknowledgements: This work was supported in part by the National Science Foundation under award number 1839191-ECCS. The authors thank Paul Kwiat, Ruichao Ma, Christian Reimer, Simeon Bogdanov, and Cristian Cortes for valuable discussions.

Author contributions: P.I. developed the idea and designed the experiment. P.I., N.B.L, and M.S.A. performed the experiments with help from D.E.L. P.I., M.S.A., N.B.L, and A.M.W. carried out the theoretical work, analyzed the data, and prepared the manuscript. A.M.W. supervised the project.

Competing interests: The authors declare no competing interests.

Data availability: The data and analysis codes used in this study are available from the corresponding author upon request.

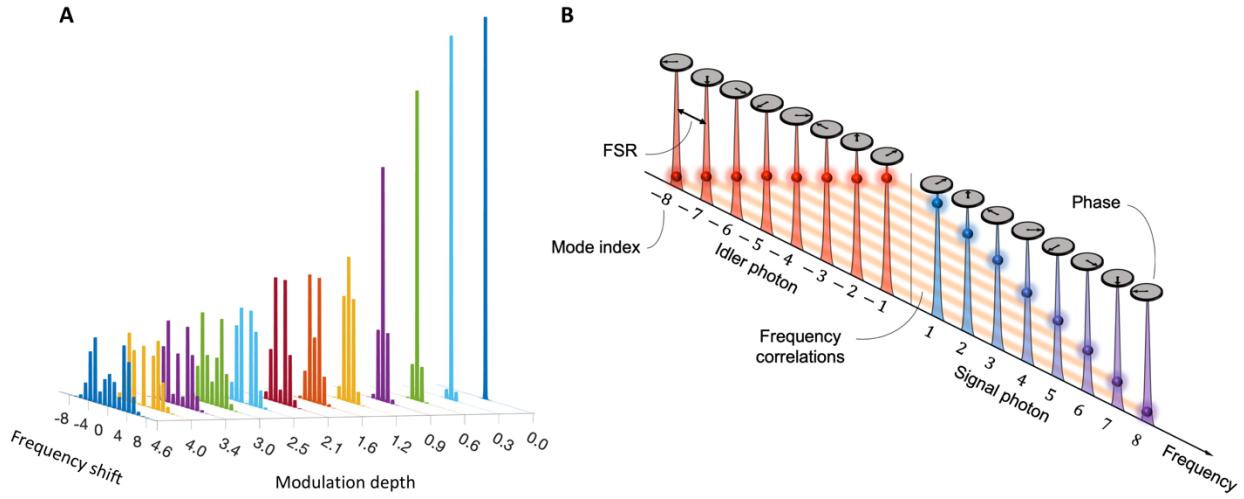

Fig. 1. Frequency domain mode splitting and biphoton frequency comb. a, Experimental data showing the effect of phase modulation on a single frequency mode for various modulation depths. These spectra were acquired with classical light but also serve as an illustration of how each single mode, even in the quantum regime, is scattered by a phase modulator. The modulation speed was chosen to match the mode separation in our quantum source and, therefore, frequency shifts are presented in terms of the BFC mode index. **b,** Illustration of a biphoton frequency comb (BFC) in frequency space. Each photon of the entangled pair is in a superposition of eight distinct frequency modes with pairwise correlations about center of the biphoton spectrum. This two-photon state has the form $|\psi\rangle = 1/\sqrt{8}\ \sum_{m=1}^{8}|m,-m\rangle_{\mathrm{SI}}$ and orange lines in the figure highlight correlations between each frequency pair $|m,-m\rangle_{\mathrm{SI}}$. A pulse shaper is used to manipulate the phase on each frequency mode prior to the quantum walk.

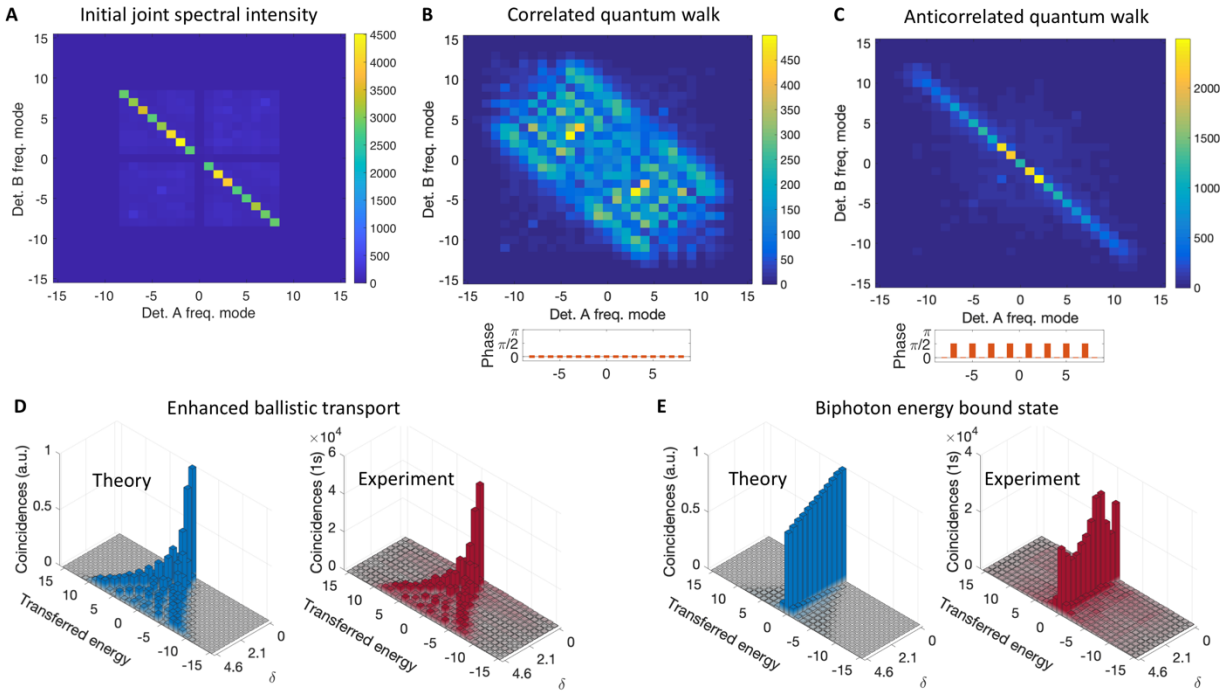

Fig. 2. Correlated and anticorrelated two-photon quantum walks a, A measurement of the joint spectral intensity (JSI) for an eight-dimensional biphoton frequency comb (BFC) of the form $|\psi\rangle = 1/\sqrt{8}\ \sum_{m=1}^{8}|m,-m\rangle_{\mathrm{SI}}$ prior to the quantum walk. Coincidences are observed for mode pairs m, $-m$, which are anticorrelated in frequency. The JSI is symmetric about the diagonal as any two-photon event $|i,j\rangle_{AB}$ is equivalent to its mirror $|j,i\rangle_{AB}$. Diagonal terms $|i,i\rangle_{AB}$ were measured by splitting frequency mode i between detector channels A and B, and are measured after all the off-diagonal elements. The acquisition time for diagonal elements was twice as long since there is a 50% probability that both photons end up at the same detector and, consequently, fail to register coincidences. **b,** JSI for a BFC after a quantum walk for the case when no additional phase is applied prior to the walk ($|\psi\rangle = 1/\sqrt{8}\ \sum_{m=1}^{8}|m,-m\rangle_{\mathrm{SI}}$). This results in two-photon events where mode indices move in the same direction, i.e., we have bunching of photons in energy space. **c,** Antibunching (mode indices of two-photon events move in opposite directions) is observed when adjacent modes start out with a π phase difference relative to one another ($|\psi\rangle = 1/\sqrt{8}\ \sum_{m=1}^{8} e^{im\pi}|m,-m\rangle_{\mathrm{SI}}$). **d, e,** Energy transferred from the phase modulator to the total biphoton state. The correlated quantum walk exhibits ballistic energy transport and we see strong energy confinement for the anticorrelated walk. The JSI for each step, or each increment to the modulation depth, is shown in supplementary material. Energy transfer in these plots is presented in units of $h\nu$ where $\nu = 25$ GHz ($h\nu = 1.656 \times 10^{-23}$ J). The variation in the coincidence rates shown in **e** is due to fluctuations of the photon flux in our entangled pair source. All the JSI elements are coincidences measured in 1 second.

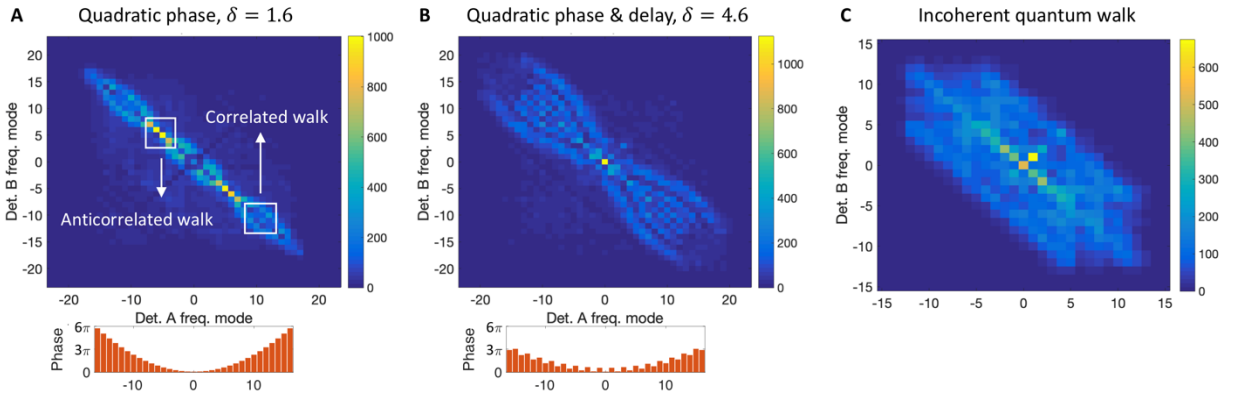

Fig. 3. Two-photon quantum walks with quadratic and incoherent input phase a, The application of quadratic spectral phase (equivalent to 1800 m of single mode fiber) to a 16-dimensional BFC results in energy subspaces with either correlated or anticorrelated walking character. The lower applied modulation depth compared to previous JSIs results in smaller diagonal spreading in the correlated subspaces. The low coincidence rate along the diagonal, relative to neighboring pixels, is an artifact of drift in the pump-to-PPLN coupling efficiency. As all diagonal elements are acquired in consecutive measurement windows, the onset of drift in photon flux during this measurement interval makes such drift noticeable along this axis. **b,** Results for a walk similar to that in **a**, but with higher modulation depth and smaller quadratic phase (equivalent to 900 m of single mode fiber). An additional linear phase was applied to ensure energy confinement at the center of the JSI, with the transition from anticorrelated to correlated character occurring further away along the antidiagonal. **c,** Simulation of a quantum walk for a mixed state that has the same initial JSI as the state in **a**. There is no indication of either ballistic energy transport or energy confinement, pointing to a clear distinction between correlated and entangled quantum walks. All the JSI elements are coincidences measured in 1 second.

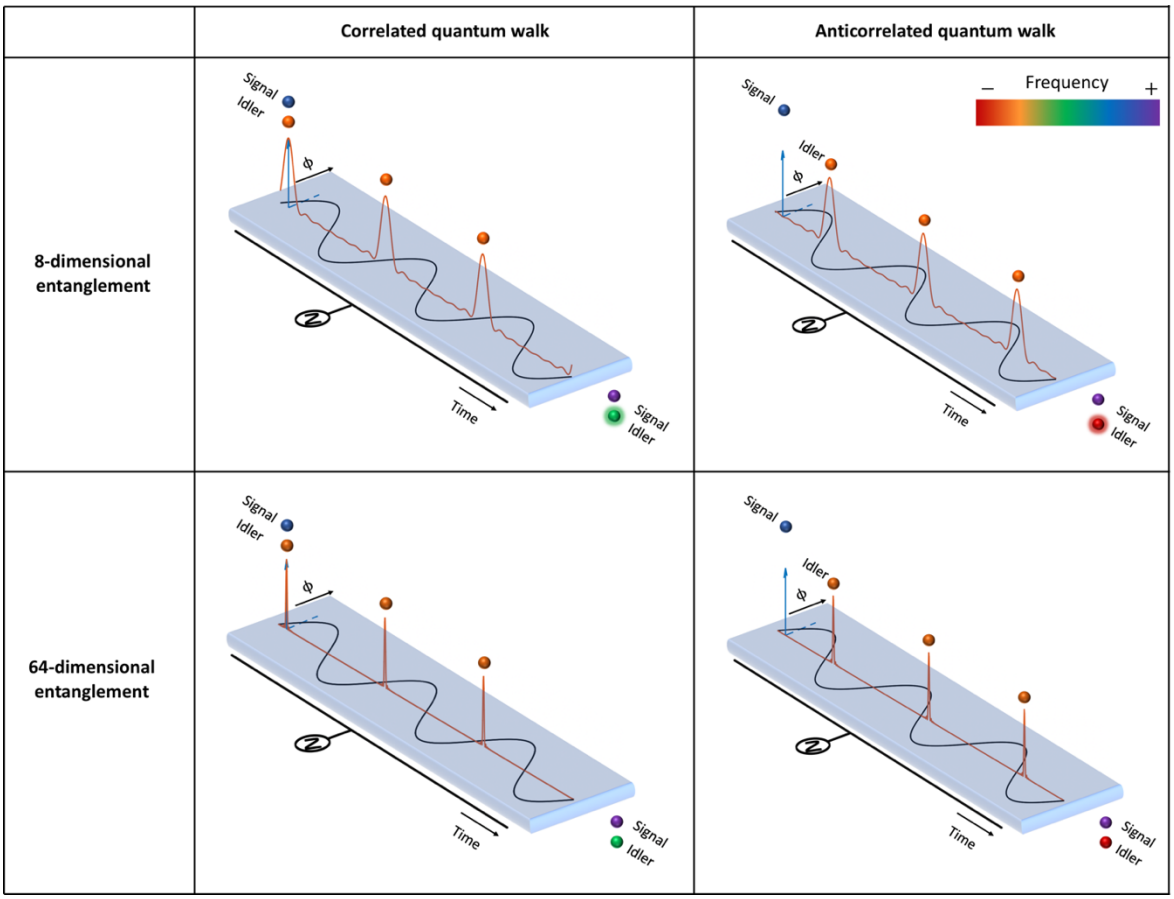

Fig. 4. Time-domain illustration of phase modulation for four different conditions (correlated/anticorrelated quantum walk, 8-dimensional/64-dimensional entanglement). The strength of the modulating RF waveform is shown with the black sinusoid. A signal photon (blue arrow) arrives at the modulator at random times owing to the nature of the photon pair generation process. However, the arrival time of the idler photon is highly correlated with that of the signal photon and is characterized by a distribution of joint arrival times that repeats at multiples of the BFC free spectral range. Since the spacing between the comb lines in the BFC is set to match the modulation frequency, the period of pulse-like features in the BFC time correlation function matches the period of the driving RF waveform. As the number of frequency modes across which the photons are entangled increases, the tighter the distribution of arrival times becomes. In the correlated walk where no phase is applied to the initial state, relative timing between signal and idler photons reduces to an integer multiple of the modulation period. Consequently, both photons in a pair experience the same frequency shift, which results in enhanced ballistic energy transport. Conversely, in the anticorrelated walk, when there is a relative π phase difference between adjacent modes, the relative timing between signal and idler photons is instead centered at an odd half-integer multiple of the modulation period. The net effect is that photons in a pair experience equal, but opposite, frequency shifts, forming a biphoton energy bound state. The change in the color of output photons reflect their frequency shifts. The cloud around the idler photon in the 8-dimensional entangled case illustrate the wider range of possible frequency shifts due to wider time-correlation function pulse features.

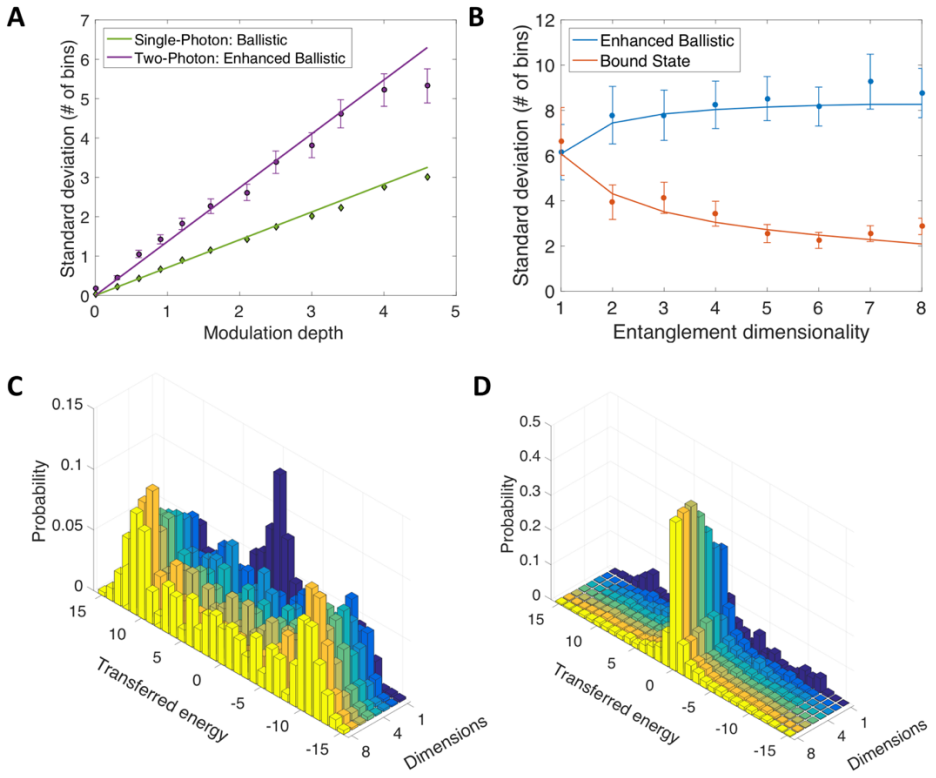

Fig. 5. Effects of entanglement dimensionality on quantum walks. a, Standard deviation of single- and two-photon energy transport. In particular, the two-photon case considers an eight-dimensional, maximally entangled photon pair. Experimental data (purple and green markers) is plotted alongside results expected from theory (solid lines). Plot points are extracted from results Figs. 1a, 2d. The standard deviation grows linearly with modulation index in both cases. However, the slope is roughly twice as steep for the two-photon case. **b,** Standard deviation of the energy transfer (output mode) distribution as a function of entanglement dimensionality for the case of enhanced ballistic transport and energy confinement when $\delta = 6.1$. Theoretical predictions are represented by solid lines and the markers correspond to experimental data extracted from **c, d**. In **a, b**, the standard deviation is computed after background subtraction (coincidence-to-accidental ratio ~ 50) and the error bars are calculated assuming Poissonian statistics. The error bars for single-photon energy transport in **a** are not shown since the experiment was carried out using classical light. **c, d,** Energy transferred to the biphoton as a function of entanglement dimensionality for enhanced ballistic transport and the bound state, respectively (see supplementary material for JSIs corresponding to each dimensionality). In **c**, the "rabbit ears" grow as the entanglement dimensionality increases, resulting in a slight increase in standard deviation, as shown in **b**. In **d,** increasing entanglement dimensionality reduces occurrence of any net energy transport between the modulator and the BFC. Consequently, frequency correlations remain confined to the constant energy axis, i.e., the antidiagonal of the JSI shown in Fig. 2c, for example.

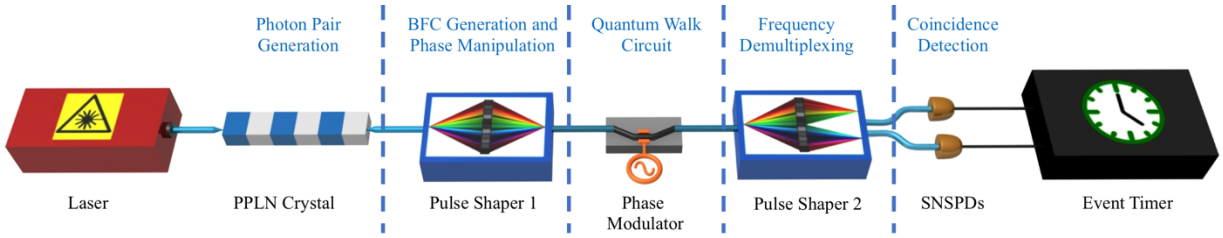

Fig. 6. The experimental setup. Broadband time-frequency entangled photon pairs are generated from a continuous-wave laser shining on a PPLN crystal. A BFC is then carved from this continuous spectrum with pulse shaper 1. Pulse shaper 1 can also manipulate the phase of each frequency mode. The high-dimensionally entangled photon pairs then enter the quantum walk circuit, namely a phase modulator driven with a sinusoidal RF waveform whose frequency is identical to the frequency spacing between the adjacent modes of the BFC. After the quantum circuit, two pulse shaper 2 selects two frequency modes at a time and send them to two SNSPDs, where correlations between the two modes are measured.

Supplementary Material:

Quantum walk Hamiltonian

A phase modulator multiplies the wavefunction of an input by $e^{i\delta \sin \omega_m t}$, which can be rewritten as $\sum_{n=-\infty}^{\infty} J_n(\delta) e^{in\omega_m t}$. Therefore, in the Fourier domain, the Hamiltonian of the phase modulation process in terms of creation and annihilation operators can be written as:

$$H = \sum_{n=-\infty}^{\infty} J_n(\delta)\, a_{m+n}^{\dagger}\, a_m \quad (1)$$

Which transfers frequency mode m to mode $m+n$ with probability amplitude $J_n(\delta)$, Bessel function of n-th order with modulation depth δ. Given the symmetry equation between positive- and negative-order Bessel functions $J_{-n}(\delta) = (-1)^n J_n(\delta)$, Eq. (1) can be rewritten as:

$$H = J_0(\delta) a_m^{\dagger}\, a_m + \sum_{n=1}^{\infty} J_n(\delta) \left(a_{m+n}^{\dagger} + (-1)^n\, a_{m-n}^{\dagger}\right) a_m \quad (2)$$

In our experiments, this Hamiltonian operates on a maximally entangled d-dimensional bipartite state of the form:

$$|\psi\rangle_{in} = \frac{1}{\sqrt{d}} \sum_{m=1}^{d} e^{i\theta_m}\; a_m^{\dagger}\, a_{-m}^{\dagger} \quad (3)$$

Where θ_m is the phase associated with state of the photon pair in modes m and $-m$. The state at the output of the quantum circuit is then the Hamiltonian acting on both signal and idler photons of the input state, resulting in:

$$|\psi\rangle_{out} = H|\psi\rangle_{in} = \frac{1}{\sqrt{d}} \sum_{m=1}^{d} e^{i\theta_m} \sum_{n,n'=-\infty}^{\infty} J_n(\delta)\, J_{n'}(\delta)\; a_{m+n}^{\dagger}\, a_{-m+n'}^{\dagger} \quad (4)$$

The probability amplitude of getting a coincidence at the output modes i and j, whose absolute value is measured in our joint spectral intensity measurement, can be interpreted with renaming the indices of annihilation operators:

$$\left|\psi_{j,k}\right\rangle_{out} = \frac{1}{\sqrt{d}} \sum_{m=1}^{d} e^{i\theta_m} \left[J_{j-m}(\delta)\, J_{k+m}(\delta) + J_{k-m}(\delta)\, J_{j+m}(\delta)\right] a_j^{\dagger} a_k^{\dagger} \quad (5)$$

The coincidences measured between modes i and j are:

$$C_{j,k} = \left\langle\psi_{j,k}\middle|\psi_{j,k}\right\rangle_{out} = \frac{1}{d}\left|\sum_{m=1}^{d} e^{i\theta_m} \left[J_{j-m}(\delta)\, J_{k+m}(\delta) + J_{k-m}(\delta)\, J_{j+m}(\delta)\right]\right|^2 \quad (6)$$

Now we consider a couple of special cases. On the antidiagonal terms, where $k = -j$, the coincidences are:

$$C_{j,-j} = \frac{1}{d}\left|\sum_{m=1}^{d} e^{i\theta_m}\left[J_{j-m}(\delta)\,J_{-j+m}(\delta) + J_{-j-m}(\delta)\,J_{j+m}(\delta)\right]\right|^2 \quad (7)$$

And using the symmetry of Bessel functions:

$$C_{j,-j} = \frac{1}{d}\left|\sum_{m=1}^{d} e^{i\theta_m}\left[e^{i\pi(j-m)}J_{j-m}^2(\delta) + e^{i\pi(j+m)}J_{j+m}^2(\delta)\right]\right|^2 \quad (8)$$

In the case of the anticorrelated quantum walk, $\theta_m = m\pi$, which results in:

$$C_{(j,-j)_{antisymmetric}} = \frac{1}{d}\left|e^{i\pi j}\sum_{m=1}^{d}\left[J_{j-m}^2(\delta) + J_{j+m}^2(\delta)\right]\right|^2 = \frac{1}{d}\left|\sum_{m=1}^{d}\left[J_{j-m}^2(\delta) + J_{j+m}^2(\delta)\right]\right|^2 \quad (9)$$

In Eq. (9), the relative phases between different states drop out, resulting in constructively interfering probability amplitudes in the anticorrelated quantum walk for the antidiagonal terms, confirming the antibunching process observed in Fig. 2c.

Energy transfer

In Figs. 2d,e, we plot raw coincidences for each energy transfer index as a function of modulation depth. This method of presentation captures all the fluctuations in our experiment, which are more visible in Fig. 2e. Another approach to present the data is to normalize each JSI by the number of total coincidences for every modulation depth [Fig. S1]. The fluctuations in the energy bound state case are noticeably reduced compared to Fig. 2e.

Incoherent quantum walk

Here, we show the simulated and experimental data for the incoherent quantum walk. To retrieve the JSI of an incoherent correlated state, we pick two correlated bin pairs $|m,-m\rangle_{\mathrm{SI}}$ for $m = 1,\ldots,8$ at a time and measure the output JSI. We then add these JSIs incoherently, which in equivalent to adding the probabilities of each output state incoherently not adding probability amplitudes (Fig. S2). Note that sharp structure evident in quantum walks of photons corresponding to coherent superpositions of frequency bins is no longer observed.

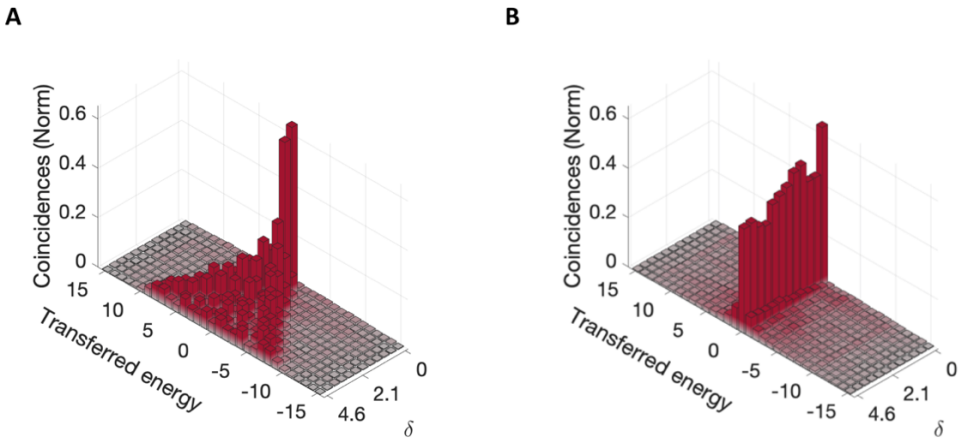

Fig. S1. Normalized transferred energy. The energy transfer for correlated **(a)**, and anticorrelated **(b)** quantum walks normalized by the number of total coincidences for each biphoton correlation map.

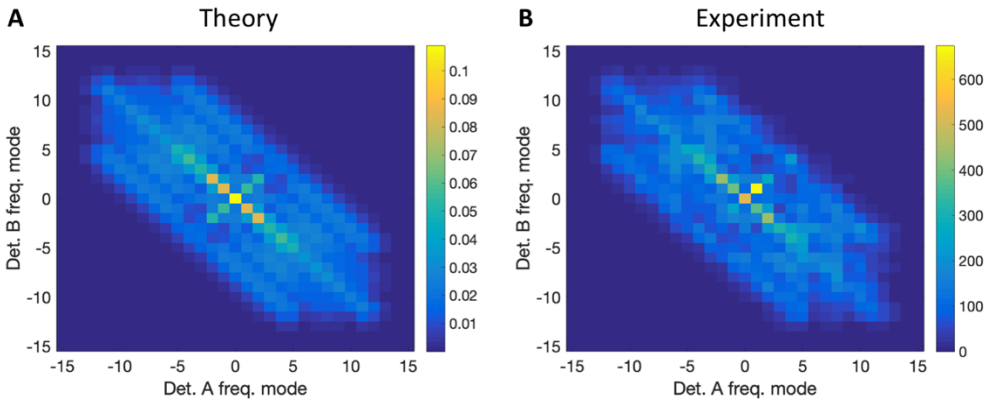

Fig. S2. Adding the output JSIs of states $|m, -m\rangle_{SI}$ for $m = 1, \ldots, 8$. The addition of the results is equivalent to the output of an incoherent mixture of correlated frequency pairs. The experimental results (**a),** match with theoretical simulations (**b)**.

Quantum walk in the limit of high modulation depth

The distinction between the quantum walk distribution of the correlated, anticorrelated, and the incoherent case becomes more evident when looking at the JSI (Fig. S3) in the limit of high modulation depth (δ=200). The correlated walk spreads diagonally while anticorrelated walk spreads antidiagonally, resembling quasi-bosonic bunching and quasi-fermionic antibunching behavior, respectively. Furthermore, by setting the linear spectral phase of the input biphoton state to a slope of $\pi/2$, we observe quasi-anyonic behavior (Fig. S3c).

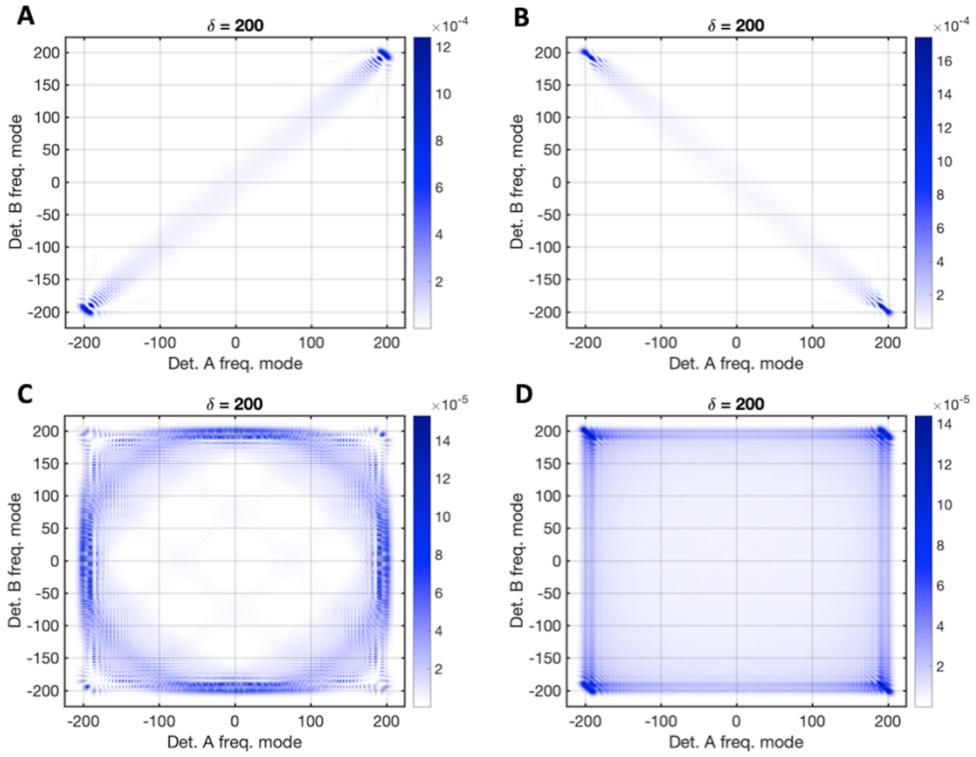

Fig. S3. Output JSI in the limit of high modulation depth (δ=200). a, correlated, **b,** anticorrelated, **c,** uncorrelated energy transfer and **d,** incoherent case, all simulated. **a,** and **b,** in the limit of high modulation clearly show bunching and antibunching effects, respectively, whereas in **c,** the biphotons relative delay is *quarter*-integer multiple of the modulation period resulting in a quasi-circular pattern. In **d,** the photons are less correlated with each other.

Movies

In the attached movies, we show theoretical and experimental JSIs for various cases. Each experimental JSI shows coincidences for one second acquisition time at each pixel of the JSI plot. The movies consist of:

1. JSI of correlated quantum walk for an eight-dimensional entangled state as a function of modulation depth.
2. JSI of anticorrelated quantum walk for an eight-dimensional entangled state as a function of modulation depth.
3. JSI of each state $|m, -m\rangle_{\mathrm{SI}}$ as a function of $m = 1, \ldots, 8$. The addition of these JSIs result in the incoherent quantum walk result shown in Fig. S2.
4. JSI of correlated quantum walk for a fixed modulation depth ($\delta = 6.1$) as a function of entanglement dimensionality.
5. JSI of anticorrelated quantum walk for a fixed modulation depth ($\delta = 6.1$) as a function of entanglement dimensionality.